UNIVERSITÀ DEGLI STUDI DI VERONA

Department of Surgery, Dentistry,

Paediatrics, and Gynaecology

Doctoral Programme in Clinical and

Experimental Biomedical Sciences

XXXVI cycle/year

Both spectral imaging and histological measurements provide a consistent evaluation of burn wound depth —A prospective, single-center, parallel-design clinical study

S.S.D. BIO 17-MED50

Coordinator: Prof. Giovanni Targher

Tutor: Ass. Prof. Ilaria Pierpaola Dal Prà

Doctoral Student: Dott. Jun Wu

Both spectral imaging and histological measurements provide a consistent evaluation of burn wounds depth— A prospective, single-center, parallel design clinical study – Jun Wu

PhD thesis

Verona, 3 December 2023

ISBN *****

Sommario

Questo articolo esplora la possibilità di diagnosticare in modo preciso la profondità della necrosi tissutale nelle ferite da ustione, con una particolare enfasi sull'utilizzo della tecnologia di imaging spettroscopico nell'infrarosso prossimale. Lo scritto sostiene che questa tecnologia consente di misurare con precisione lo spessore del tessuto necrotico nelle ferite da ustione. Per valutare la sua efficacia, è stato condotto uno studio clinico nel periodo compreso tra il settembre 2020 e il maggio 2023, coinvolgendo pazienti ustionati ricoverati presso il Dipartimento di Chirurgia Plastica e delle Ustioni del Primo Ospedale Affiliato dell'Università di Shenzhen.

L'autore specifica che per questo studio ha impiegato sette diversi modelli di calcolo. Egli ha così determinato che un modello di regressione Adaboost basato sulla "*principal component analysis*"(PCA) ha fornito i risultati più favorevoli. Questo modello ha impiegato immagini con un minimo di falsi colori e ha fornito risultati con un alto livello previsto di precisione. Inoltre, tale modello ha dimostrato di possedere accuratezza e stabilità, avendo una prevista deviazione standard dei risultati inferiore ai 50 μm nell'intervallo di profondità del tessuto necrotico compreso tra i 200 μm e i 600 μm.

Tuttavia, l'autore riconosce a tale modello un limite nella previsione e precisione dei risultati per ustioni di profondità per inferiori ai 200 μm o superiori ai 600 μm, il che indica la possibilità di ulteriori miglioramenti. La presente ricerca sottolinea le potenzialità della tecnologia di imaging spettroscopico nell'infrarosso prossimale per determinare con precisione la profondità delle ferite da ustione, offrendo un promettente avanzamento nel campo della precisione della diagnosi e del trattamento delle ustioni. Inoltre, lo studio in evidenzia la necessità di ampliare le dimensioni del campione per migliorare l'accuratezza della valutazione della profondità delle ustioni.

Abstract

Background: Burn wound management is still a significant challenge, particularly in relation to the control of scar formation and contracture that lead to bodily deformity and dysfunction. Saving alive tissue as much as possible when debridement of burn wounds will upkeep the tissue volume and thus promote a better tissue regeneration, external appearance, and function. Unfortunately, it is difficulty to precisely distinguish the necrotic and alive tissue by eyesight only. Therefore. a precise debridement is almost impossible to perform. Several strategies focusing on an objective evaluation of burn depth according to the wound's local circulation have been developed. However, s none of them directly evaluates the burn depth that is critical for a precise debridement as well as for a better regeneration of the wound. Herein, we show that our invented near-infrared spectral imaging device and its technology are promising tools allowing to measure the necrotic tissue thickness in burn wounds.

Method: Based on our previous in vitro and in vivo studies, I designed a prospective, single center, clinical study on burn depth evaluation by means of near-infrared spectral imagining device in parallel to control histological measurements . To this aim, the burnt patients admitted to the Department of Burn and Plastic Surgery of the First Affiliated Hospital, Shenzhen University, from September 2020 to May 2023 were recruited. The near-infrared spectral signals were collected from target areas of different burn depths selected by senior burn surgeons, which were subsequently biopsied. Masson staining was used for histological measurements of burns depth that served as standards. The validity was assessed of seven calculating models, i.e., Linear Regression, Kernel Ridge Regression, Random Forest Regression, Gradient Boosting Regression, Decision Tree Regression, Extra Trees Regression, and AdaBoost Regression. Two thirds of the spectral data served as the training data set, while the remain in gone third made the test data set.

Results: A total of 53 patients with 171 wounds were analyzed. An Adaboost regression model based on principal component analysis (PCA) was proven to be the best one being endowed with minimal false color imagery, while highlighting an elevated level of prediction accuracy. Notably, the standard deviation of the model's prediction results was less than 50 μm in a necrotic tissue depth range between 200

μm and 600 μm, a sign of its accuracy and stability. However, the predictive accuracy of the model was less favorable when burn depth was less than 200 μm or more than 600 μm.

Conclusions： This study highlights the potential of near-infrared spectrum (NIR) imaging technology in accurately determining the burn wounds depth. It represents a significant step forward in the quest for precision in wounds diagnosis and treatment.

Limitations： The patients' sample size needs to be increased further. Theoretically, more samples will provide a greater precision of burn depth evaluation.

Key words

Burn depth, near-infrared spectrum imaging, AdaBoost Regression, precision wound diagnosis, training data.

Index page

Introduction

1. Significance

The human skin covering the body surface is the largest organ, being endowed with immune, nervous, endocrine functions, as well as crucial activities such as secretion, absorption, excretion, temperature regulation, and electrolyte balance. The skin plays a key role in maintaining the unity of the body's internal environment separating it from the surrounding environment [1]. Burn wounds can seriously damage the structure and functions of the skin, and cause critical complications such as electrolyte imbalances and infections. Therefore, an early, precise diagnosis is crucially needed for proper burn wound treatment [2].

Available research data indicate that a timely and accurate assessment and treatment of burn wounds can effectively reduce the speed and extent by which superficial burns might turn into deep burns. This approach can save lives, prevent complications, promote wound healing, and accelerate the recovery process [3]. Therefore, a prompt and accurate determination of burn wounds' depth is essential for maximizing the preservation of skin appendages, laying the foundation for high-quality wound healing, and reducing proliferative scar formation. Establishing new concepts, techniques, and equipment for precise diagnosis of burn wounds is a significant undertaking in the field of surgery.

In recent years, rapid advancements in various physical technologies and their successful applications in Bio-medicine have provided the theoretical guidances and practical possibilities to achieve "early," "accurate," and "rapid" diagnosis of burn wound depth.

2. Current status and progresses in burn depth evaluation

2.1 The depth evaluation of burn wounds is still empirical

Determining the depth of necrotic tissue in a burn wound is the initial most critical step in the clinical treatment of burnt patients. Currently, burns grading and classification still rely on subjective clinical experience, including factors such as wound color, texture, moisture, and hair plucking tests [4, 5]. Research has shown

that in judging burn wound depth even the most experienced burn surgeons achieve an accuracy rate of only about 70% [6,7]. The existing clinical experience-based methods quite accurately distinguish extremely deep and superficial burn wounds using the current third-degree four-point or fourth-degree five-point system. However, mixed second-degree burn wounds still represent a significant challenge for clinical decision-making, which impacts the choice between a conservative treatment and a surgical intervention [8]. Thus, reaching a precise clinical judgment for mixed second-degree burn wounds remains an exceedingly difficult task.

Since the 1960s, various emerging technologies, such as fluorescence detection , laser Doppler, near-infrared thermal imaging, multi-spectral imaging, etc., have been used to attain a clinical diagnosis of burn wound depth. Indeed, some of them deserve to be shortly mentioned here.

Laser Doppler Imaging (LDI): LDI is the only FDA-approved device for assessing burn wounds depth. It is based on the principle that when a laser light encounters moving objects (mainly blood cells) in a burn wound, it produces a Doppler frequency shift. By analyzing this frequency shift, one can detect the flow of blood cells within burnt tissues [9,10]. LDI distinguishes the depth of burns on the ground of existing differences in blood flow speed between superficial and deep wounds [11]. However, LDI indirectly assesses the degree of burnt tissue damage by measuring its perfusion but cannot directly evaluate the necrotic tissue depth.

Spatial-Frequency Domain Imaging (SFDI): SFDI is a wide-field imaging technique based on the principle of diffuse reflectance. It can analyze collagen denaturation, blood flow, and blood vessel damage in burn wounds, distinguishing different degrees of burn injury [12,13]. While this technology has significant potential in burn wound diagnosis, it has been the object of only a limited number of reports. Therefore, further experiments and observational data are needed to support its diagnostic effectiveness in the burns field.

Laser Speckle Imaging (LSI): LSI measures blood cell flow velocity by detecting dynamic laser speckle effects. Unlike LDI, LSI can provide real-time imaging of the entire field of view, effectively controlling errors caused by small movements [14,15]. However, like LDI, LSI indirectly assesses through tissue

perfusion the degree of burn wound damage but cannot directly evaluate the necrotic tissue depth [16].

Optical Coherence Tomography (OCT): OCT projects light onto target tissues, and the light reflected from their different layers is used to create digital signals that display the micro-structure of the illuminated tissues [17,18]. Recent reports suggest that OCT-based vascular imaging can assess burn wound depth on the basis of depth-related factors, such as blood vessels, edema, and tissue damage [19]. However, OCT has a restricted field of view, less than 1 cm^2, which limits its practical application in burn wound diagnostics [17,20].

Infrared Thermal Imaging Technology(*ITIT*): This method indirectly evaluates burn wound depth by detecting the different thermal radiations from the skin in the burnt area [21]. Studies have shown that the temperature of superficial second-degree burn wounds rises, while that of deep second-degree burn wounds can decrease by 1-3 °C, while full-thickness necrotic burn wounds exhibit a grater than 3 °C temperature drop. However, the precision of this method is affected by various environmental and operational factors, which lead to significant errors and prevent an accurate wound depth assessment [22].

Fluorescence Detection Technology (FDT): This method entails the injection of fluorescent compounds, such as indocyanine green (ICG), into the bloodstream [23]. Different excitation lights are used to evaluate the wound necrosis deon the basis of the intensity, peak size, and temporal characteristics of the fluorescence emitted from the wound [24]. However, substances applied to the wound, such as medications and dressings, can significantly affect the accuracy of ICG detection [25]. Additionally, like other techniques, FDT indirectly assesses the degree of burn wound damage through tissue perfusion but cannot directly evaluate the necrotic tissue depth.

Ultrasound S*canning Technology (UST)*: UST was first proposed to assess burns depth in 1974. It primarily identifies the boundary between viable and necrotic tissues by revealing the differences in echogenicity between normal and burnt skin [26,27]. However, UST requires a direct contact of the scanner with the wound, increasing the risk of propagating wounds cross-infections . Additionally, current ultrasound measurements have poor accuracy, cannot achieve micrometer-

level diagnostics, and rely on the experience and skills of ultrasound technicians to identify the necrotic boundaries between normal and burnt skin [28,29].

Terahertz Imaging Technology (THz): THz utilizes the dielectric properties of the water present inside tissues [30], as its reflectance variance is proportional to the water tissue content. Thus, to diagnose burn wound depth, THz imaging primarily relies on the edema amount within the wound [31,32]. Similarly to other techniques, THz indirectly assesses the degree of burn wound damage but cannot directly evaluate the necrotic tissue depth.

In short, the above mentioned techniques rely on factors such as blood flow speed, temperature, edema, and other wound components to indirectly assess the degree of burnt tissue necrosis, without directly determining the necrotic tissue extension. As a result, these techniques allow to classify wounds but cannot directly diagnose the necrotic tissue depth, thereby failing to meet the clinical demand for an accurate determination of necrosis depth in burn wounds.

2.2 Current development of spectral imaging technology (SIT)

In recent years, SIT has shown immense potential due to advancements in equipment performance, spectral analysis methods, and algorithm technology, offering new avenues for burn wound diagnosis. SIT supplies "spectral fusion" (spectrum/image) data in the ultraviolet, visible, near infrared, and mid-infrared regions of the electromagnetic spectrum. Different tissues have distinct spectral signatures due to their nonidentical constituents. Hence, SIT can distinguish the different components of target tissues by taking advantage of their various spectral signals. Initially, SIT was applied to satellite remote sensing and space exploration. Nowadays, its application has been expanded to various fields, including medical diagnosis, agricultural inspection, forestry surveys, and cultural heritage identification [33,34,35].

Widely used SIT systems come in diverse types, such as filter wheels, dispersion, and interferometry equipments [36]. Filter wheel-based SIT systems have fewer spectral bands and lower spectral resolutions. Dispersive SIT systems offer higher spectral resolution but a lower energy efficiency, which leads to an

inadequate detection of weak signals. Interferometric SIT systems have higher energy efficiency and sensitivity but suffer from insufficient spatial resolution and complex optical structures. Additionally, most of these SIT systems occupy large volumes due to their structural complexity, and hence are not suited for adaptability and portability.

As far back as the 1990s, German clinicians used three bandwidth filters (red, green, and blue) to diagnose the depth of skin burns [37]. However, due to the narrow bandwidth of the filters, the information obtained through this technique was not enough to allow for the identification of necrotic tissue . With its development SIT's applications have been gradually extended to fields such as Dermatology and Neurosurgery. SIT now covers the visible and near-infrared wavelength ranges, thereby achieving some targets in clinical applications [38,39,40]. For example, the Dutch company Herke conducted an experimental study using a compact liquid crystal SIT system as a diagnostic tool for Dermatology and Neurosurgery. The results showed that spectral imaging technology can supply detailed spectral information when detecting subtle changes in skin tissue structure. However, the spectral resolutions and spectral ranges of the existing SIT systems are not sufficient to identify the necrotic skin tissue and obtain images of its layers. To bring medical SIT systems to clinical application, the core challenge is whether high-resolution, narrowband, wide-spectrum liquid crystal tunable filters (LCTFs) will be successfully developed.

However, achieving high-resolution, narrowband, wide-spectrum liquid crystal SIT poses several technical challenges. Firstly, increasing the number of liquid crystal filters to achieve narrowband spectral scannings significantly decreases the device transmission intensity, leading to lower spectral imaging quality. Secondly, increasing the number of liquid crystal filters also reduces the field of view, making it impossible to examine large burn areas. Thirdly, the device is rather sensitive to external temperature changes, which cause a shift in the center wavelength during scanning that is detrimental to correct spectral recognition. Therefore, achieving high-resolution, narrowband, wide-spectrum liquid crystal SIT imaging presents new challenges for current liquid crystal SIT, liquid crystal

SIT device processing technology, and liquid crystal SIT material synthesis technology.

After a decade of team efforts, we have developed a SIT device called DEPS-IS-1A (Deps Medical Technology Co., Ltd.). This instrument achieves spectral imaging of incident light in the 900 nm-1700 nm wavelength range. It offers a spectral resolution of about 10 nm, thereby enabling the exact identification of necrotic skin tissue. We have conducted preliminary tests on *ex vivo* and in vivo animal burn wounds, and our results have shown an excellent identification performance and promising prospects for detecting burn wounds' necrosis depth [41,42,43,44].

3. Purpose of the study

It was my aim to set up a novel approach entailing near-infrared spectral imaging allowing for objectively measuring the absolute values of burn depths.

4. The characteristics, structural composition, and mechanism of function of the novel spectral imaging device

4.1 Device general characteristics

The novel spectral imaging device is based on a liquid crystal adjustable filter, which has the advantages of fast wavelength switching, wide working spectrum, high spectral resolution, small size, low power consumption, effortless operation, etc., and hence can acquire and process high-resolution spectral images.

4.2 Spectral imaging device structure composition

The novel spectral imaging device consists of a special illumination stand with sample table, illumination light source, optical lens, spectral camera, spectral image acquisition software, spectral image analysis software, power supply module, and related connection cables.

4.3 Functioning mechanism

The spectroscopic technique uses the back scattering of the infrared part of the spectrum for burn wounds evaluation. The basic principle is to analyze the different

degrees of attenuation of the characteristic spectrum after the absorption of near-infrared light by the tissues in the burnt area. This allows to calculate the necrotic tissue depth is calculated and to artificially color it.

Materials and Methods

1. Materials

1.1 Reagents

Table 1. Reagents used in the experiments.

Name	*Source*
Masson tricolor staining solution kit	Sevier Biotechnology Co., Ltd
Xylene	Aladdin Reagents Ltd.
Anhydrous 100% ethanol	Lingfeng Chemical Reagent Co., Ltd
95% ethanol	Lingfeng Chemical Reagent Co., Ltd
Glacial acetic acid	Chemical Reagent Factory
Paraformaldehyde	Biosharp

1.2 Equipment

Leica (HistoCore PEARL) fully automatic tissue dehydration machine.
Leica (HistoCore PEARL) paraffin embedding machine.
Thermo Fisher (HM340E) semiautomatic rotary paraffin microtome.
DEPS (DEPS-IS-1A) novel medical spectral imaging device.

Figure 1. Picture of the medical spectral imaging device.

2. Study Design

Consistent evaluation of burn depth by both spectral imaging and histological measurements: a prospective, single-center, parallel design clinical study.

2.1 Patients' personal basic information

The following information was recorded for all recruited patients.

- Demographics: age, sex, height, weight, BMI, race.
- Medical history: past and present history of illnesses, allergies, and compound injuries (e.g., traumatic brain injury, inhalation injury, fracture, etc.)
- Body surface burns: type of burn, cause of burn (hot fluid, flame, thermal contact, etc.), anatomical location of burn, total burn area (%TBSA), subjective evaluation of burn depth, transfer time from burn to burn center.
- Subjective evaluation: the clinical features of different depth burns are shown in Table 2.

Table 2. Clinical diagnosis of burn depth

Burn depth	*Clinical Features*
I degree	Localized erythema, burning pain, no blisters.
Superficial II degree	The wound surface is red, swollen, and painful, with watery scars or blains separating epidermis from dermis holding a plasma-like yellow fluid. After removal of the watery scars, the wound surface is bright red, moist and whitens with pressure on the basal tissues; the pain is more intense and there is much exudation. Positive hair plucking or prick test with severe pain sensation.
Deep II degree	After rupture of the skin with blisters or removal of the decayed skin, the trauma surface appears red-white in color or is dotted by a network of tiny embolized blood vessels, and exudes a lot of fluid; edema is obvious; nociception is dull; and the hair plucking test or pinprick test are slightly painful.
III degree	The trauma surface is scorched by pale white, yellow-white, burnt yellow or burnt black bands; dry and hard scorching bands can appear to be leather-like; the subcutaneous vein network can be seen under the scorched areas in the form of branching dendrites; the trauma surface is devoid of pain sensation;the hair plucking test is easy to conduct and is painless.

2.2 Clinical semiquantitative evaluation of local signs of burn wounds

Exudate: (-), no exudate with the innermost dressing on the wound being dry; (+). discrete amount of exudate; (++), more abundant yellowish exudate ; (+++), a lot of exudates wetting the outermost dressing layer.

Swelling: (-), no swelling, approximating normal skin aspect; (+), swelling at the trauma edges, clearly above normal skin;(++), pain and marginal swelling and/or redness, spreading around the traumatized area ; (+++), obvious spreading of puffiness or swelling (edema) around the trauma area, with dipping when swelling is pressed.

2.3 Other clinical records

All the symptoms and signs as well as laboratory tests were recorded as required by standard clinical diagnosis and treatment criteria.

2.4 Spectral imaging data collection

One doctor oversaw the collection of spectral data of the burn wounds using the DEPS-IS-1A device. When patients were anaesthetized in the operation theater, the doctor in charge cleaned the target areas using physiological solution and next dried them with a sterilized gauze. Next, the spectral imaging device was used to collect the spectral data from the targeted areas. After that, a tissue biopsy of the latter was taken for histological examination (see #2.5. below for details).

2.5 Histological measurement of burn wounds depth

After completing the preoperative preparations and anesthesia, the burn wound to be debrided was routinely disinfected and toweled, and a biopsy (ring drill) was conducted by means of a 3-mm skin biopsy device. The specimen was naturally straightened, attached to hard cardboard, and placed in 10% formalin fixative for later examination. After local gauze pressure, the burn's biopsy edge was dressed under pressure to stop bleeding.

2.6 Selection criteria

2.6.1. Patients with thermal injury (including electrical burns) with a burnt area > 1% TBSA.
2.6.2. Patients admitted to the hospital within one week following injury.
2.6.3. Patients eligible for surgical treatment (e.g., escharectomy); alternatively, patients to be treated conservatively but willing after informed consent to undergo biopsy.

2.6.4. Location of target wounds: non-facial, non-hand, non-joints other burn sites.
2.6.5. Patients who understood the aim of the test and voluntarily agreed to conduct it.
2.6.6. Patients who signed the informed consent form.

2.7 Exclusion Criteria

2.7.1. Patients with combined injuries due to specific causative factors, such as radiation lesions, chemical burns, etc.
2.7.2.Concurring presence of local or systemic diseases in the test area that affected the wound depth evaluation, e.g., diabetes combined with a skin disease), arterial occlusion or venous ulcers of the lower extremities (affecting the observation), malignant tumors, rheumatic immune diseases, other skin diseases, etc.
2.7.3. Other circumstances that the investigator considered inappropriate for participation in this study, including patients that were concurrently taking part or planning to participate in other clinical trials during the study period; patients suffering from a mental illness or being otherwise unable to give a fully informed consent.

2.8 Withdrawal from clinical study

2.8.1. *Withdrawal by investigator's decision:* When a subject who had been enrolled in the study developed during the study a condition that made it inappropriate to continue, the investigator could decide that the case should be withdrawn from the study. For example, certain comorbidities, complications, or special physiological changes occurring during the trial that hindered to continue; also, poor patient compliance during the study.
2.8.2. *Withdrawal by patient's decision:* Subjects have the right to withdraw during the course of the study, as specified in the consent form; alternatively, subjects who do not explicitly request to withdraw from the study but no longer take part in it.

The investigator should understand and document the reasons as much as possible, keep the CRF form, and transfer the last test result as the final result.

2.9 Data review and database management

2.9.1 Completion and transfer of case report forms

A case report form must be compiled for each successfully enrolled case and completed by the investigator. Each completed case report form is next reviewed by the clinical monitor and then handed over to the data manager for data entry and management.

2.9.2 Data entry and modification

The data manager verifies the data in each case report form. If he finds some doubtful data, he sends through the clinical monitor a query form to the investigator. Next, the data manager makes data corrections and/or confirmations based on the investigator's answers and if necessary may issue query forms again.

Data entry is done via a double independent input, and then a data consistency verification is conducted. This verification can be stopped only after a complete agreement is reached.

2.9.3 Data review

After data entry and inspection, the data are reviewed by the data manager, principal investigator, and statistical analyst, and the final definition and judgment of the analyzed population is thus completed.

2.9.4 Database locking

Once all the data have been entered into the database, all queries have been resolved, and the population analysis has been defined and judged, the data can be locked.

2.9.5 Data processing

The locked data are handed over to the statistical analysts for evaluation.

2.10 Statistical analyses

After the test protocol was figured out, a statistical analysis plan was developed by a professional statistician who refined and documented it prior to data lock. SAS software was used for the statistical .

Overall, EP9 A3 guidelines were followed for this statistical analysis.

Statistical description and inference of the basic data: applicable descriptive indicators and hypothesis testing methods were selected based on the characteristics of the data. The mean, standard deviation, median, minimum, maximum, and upper and lower quartiles were calculated to describe quantitative indicators, and the number of cases and percentages were used to recount categorical indicators. Depending on the distribution of the data, group comparisons of quantitative indicators were conducted by group *t*-test, ANOVA, or Wilcoxon rank sum test.Categorical indicators were compared by chi-square test or exact probability test. Finally, rank data comparisons were performed by Wilcoxon rank sum test.

Principle of consistency evaluation (PCA): The consistency analysis for the depth values from histological examinations was conducted by Bland-Altman method. The depth values of spectral test results for the main evaluation indexes, and scatter and deviation plots, correlation coefficients, and regression analysis coefficients were also used for further consistency determinations.

The difference was considered statistically significant at $P < 0.05$ bilaterally.

2.11 Analysis of data sets

2.11.1 *Consistency analysis data set*: In the first measurement, all case data of both empirical and spectral imaging test were obtained.

2.11.2 *Safety data set*: all subjects included in this study were taken into account.

2.11.3 *Baseline analysis*

A descriptive statistical analysis was conducted comparing the balance of basic information of the included subjects, such as gender, age, medical history,

weight, and other measures. Baseline and demographic information was tabulated and described. For continuous variables, descriptive results, including the number of cases, mean, standard deviation, maximum, minimum, median, and upper and lower quartiles of subjects were considered. For categorical variables, the number and percentage of subjects in each category were compared.

The resulting depth values from histological measurements and depth values from spectral tests and the results from the main evaluation indexes were analyzed for consistency using the Bland-Altman method, while scatter and deviation plots, correlation coefficients, and regression analysis coefficients were used for further consistency determination.

2.12 Main observation indicators

Consistency analysis was performed using the Bland-Altman method and ATE/LER regions with depth values as the main observation, and scatter and deviation plots, correlation coefficients, and regression analysis coefficients were also used for further consistency determination.

2.13 Calculation of sample size

According to the current guidelines of Chinese FDA for *in vitro* device studies, the total sample size of the clinical study must be no less than 200 cases. According to statistical principles, the sample size calculation process is as follows.

Based on this formula, if $\bar{d} = 0$, it can be concluded that the sample content estimation formula when the difference between the two methods is 0

$$n = \frac{(2 + z_{1-\gamma/2}^2)(t_{\alpha/2,n-1} + t_{\beta/2,n-1})^2 s_d^2}{2(\bar{d} + z_{1-\gamma/2} s_d - \delta)^2}$$

The *t*-quantile in this formula is related to the sample size and requires an iterative approach. In the first iteration, the first value of '*n*' is obtained by substituting the *t*-quantile of the standard normal distribution. The iteration process

continues until there is no significant difference between the results of the two consecutive iterations. The obtained result stands for the desired sample size.

$$n = \frac{\left[Z_{1-\alpha/2}\sqrt{P_0(1-P_0)} + Z_{-\beta}\sqrt{P_T(1-P_T)}\right]^2}{(P_T - P_0)^2}$$

Based on the above assumptions, when the mean of the difference between the two methods was 50 μm, the standard deviation was 20 μm, and the range of agreement was 100 μm, the sample size was calculated to require a total of 106 subjects.

Considering the potential shedding cases (15-20%), the total number of subjects to be enrolled should have been 130.

2.14 Handling of missing/early exit data

Missing values for the main evaluation indicators and the remaining indicators in this study were not filled.

2.15 Procedures for reporting deviations from the original statistical plan

The first draft of the statistical analysis plan was formed after the study protocol and case report form and could be revised, added to, and refined as the clinical study proceeded. It is confirmed in document form before the data lock and could not be changed thereafter.

If, during the statistical process, it became necessary to add some analyses more or even change the statistical methods due to the nature of the data, this event should have been specified in the summary report of the clinical study.

2.16 Ethical Issues and Informed Consent in Clinical Research

This clinical study was conducted in compliance with the Declaration of Helsinki and the Chinese regulations and rules about the quality management of clinical studies concerning a medical device. The study protocol was approved by

the Ethics Committee (EC) of the study unit before the study onset. Any modification of the study protocol were approved by the Ethics Committee before implementation. Serious adverse events during clinical research were sent to the Ethics Committee in writing in a timely manner.

Before each subject was enrolled in this study, it was the responsibility of the investigator to explain the study to the subject in an understandable verbal or written language and to carefully answer to the subject's questions. A written informed consent form was given to each subject prior to enrollment. It was the responsibility of the study physician to obtain an informed consent prior to each subject's entry into the study and to keep it in the study file.

This study was conducted based on the Declaration of Helsinki, the principles for the implementation of clinical research protocols (ICH-GCP, International Conference on Harmonization - Code of Practice for the Management of Pharmaceutical Clinical Research), and the relevant standing laws and regulations of the People's Republic of China.

2.17 Informed consent process and text of informed consent form

Prior to enrolling patients for this study, the responsible investigator provided them or their guardians with a complete and thorough description in writing of its purposes, procedures, and risks . Subjects were made aware that they had the right to withdraw at any time and that their personal information would be kept confidential. A written subject informed consent form was given to each subject prior to enrollment as the investigator had to obtain an informed consent prior to each subject's entry into the study and to store it in the study file.

With the Ethics Committee agreement in principle and the investigator belief that it was useful, some incapacitated subjects took part in the clinical study, once their guardian had signed the anticipated informed consent When neither the subject nor his/her guardian could read, a witness had be present during the informed consent process. After a detailed explanation, the witness had to read the informed consent form, whose contents replicated the verbal informed consent. Once the

subject or his/her guardian verbally consented, both the and the investigator's witness signed and dated the informed consent form on the same day.

2.18 Deviations from clinical research protocols

Protocol Deviation (PD): Cases that did not meet the requirements of the population to be included in the original protocol due to distinct reasons, so that the entire study process was not conducted as originally specified in the protocol.

Table 3. Severity determination of deviations from the program .

Severity Degree	Description
Mild	Visits/observations/examinations outside the time window that do not affect the subject's continued use of the study device as per the protocol or the validity of the evaluation of the primary efficacy and key secondary efficacy indicators Data missing due to missing data points or laboratory parameters seen under the protocol, but not affecting the primary efficacy or key secondary efficacy or safety index results. Incomplete observations/evaluations that did not affect primary or secondary key efficacy or safety outcomes.
Severe	Subjects that did not meet any of the inclusion criteria or met any of the exclusion criteria, yet were included in the study. Subjects that during the study met the criteria for study discontinuation but did not withdraw. Failure to examine safety indicators, primary efficacy indicators, or key secondary efficacy indicators as required by the protocol, thereby jeopardizing the scientific validity of the study. Subjects that received an incorrect treatment to the extent that it impaired subject safety or statistical analysis. Any serious violations of the GCP principles occurring during the implementation of the program

Although PD may be difficult to avoid during clinical studies and affects the authenticity and accuracy of the results, the investigator abode by the protocol approved by the Ethics Committee.

Any deviation from the protocol that occurred was documented and explained by the on site investigator using the Protocol Violation Report form provided by the sponsor, reviewed, and confirmed by the principal investigator, and then sent to the monitor/sponsor.

To prevent PD from occurring, at the time of informed consent the investigator explained to the subject the importance of adhering to the study protocol .

2.19 Acquisition of the original data

Source documents. This study employed informed consent forms, subject screening and enrollment forms, subject identification code forms, subject's laboratory checklists, device use record forms, etc. Any observation and examination results pertaining to the clinical study were promptly, accurately, completely, standardized, and faithfully recorded in the just mentioned source documents.

Source data. Source files for each enrolled subject included at least the following data: subject's name, date of birth, gender, protocol number, study device name, study screening or enrollment start date, study device use date, investigator's signature; laboratory test results and report date, and study monitor's signature.

The authorized monitor had the right to access and verify the source data/source documents of teach enrolled subject to figure out whether the investigator was conducting the clinical study in keeping with the protocol and whether the source data/source documents were recorded in the specific subject's medical record in a timely manner. The supervisor needed to confirm that the source data/source documents were traceable and verifiable. Also, the data filled in the CRF had to correspond to the source data/source documents.

Source data/source documents were all safely stored following the requirements of standing laws and regulations.

2.20 Principle of confidentiality

The researchers maintained strict confidentiality of patient information, ensuring that data presented in reports remains completely dissociated from any identifiable patient details.

2.21 Clinical research institutions and investigator responsibilities

2.21.1 The investigator responsible for the clinical study have the proper qualifications.

2.21.2 Clinical research institutions should properly keep clinical research records and basic documents.

2.21.3 The investigator ensured that the study's staff was familiar with the principles, scope of application, product performance, operating methods, installation requirements, and technical specifications of the research medical device. The staff also understood the preclinical information and safety information of the research medical device, including details about the potential risks, risks prevention, and emergency control.

2.21.4 The investigator also ensured that the investigational medical device was used only for the subjects of the clinical.

2.21.5 The investigator strictly abode by the clinical research protocol and did not deviate from or change it without the consent of the sponsor and the Ethics Committee, or without the approval of the State Food and Drug Administration in accordance with the standing regulations.

2.21.6 The investigator oversaw the recruiting of proper subjects and personally talked with them or their guardians.

2.21.7 The investigator or other personnel involved in the study did not force or otherwise improperly induced any subject to take part in the study.

2.21.8 The investigator managed making medical decisions related to the clinical study.- In any adverse event related to it the investigator also ensured that an adequate and prompt treatment and management was provided to the involved subject.

2.21.9 Also, in the rare cases of serious adverse events the investigator did at once report them in writing to the clinical research institution, and to the sponsor.
2.21.10 The investigator ensured that all the clinical study data were accurately, completely, clearly, faithfully, and promptly included in the case report form.
2.21.11 The clinical research investigator supplied all the records n related to the study, which were subjected to monitoring and verification by the sponsor and to supervision by the Ethics Committee.
2.21.12 At the end of the clinical study, the investigator ensured that all records and reports had been completed, and that the required clinical data had been delivered to the clinical research institution on time as required.

3. Sample Preparation

Skin samples (0.3 cm x 0.3 cm) were collected immediately after acquiring spectral data. The samples were fixed in 4% formaldehyde neutral solution for 24 hours.

4. Histological Processing

The dehydration, transparency, and paraffin embedding steps were performed using a Leica HistoCore PEARL automated tissue processor.

Paraffin-embedded tissue blocks were sectioned into 5 μm-thick slices using a semi-automatic rotary microtome (SaiMeiFeiSe HM340E).

Masson trichrome staining was applied to the tissue sections, involving a series of steps, i.e., *Deparaffinization and hydration*: The slides were heated at 65 °C for 1-3 hours; next they were sequentially immersed in xylene I, xylene II, 100% ethanol I, 100% ethanol II, 95% ethanol, 80% ethanol, and finally twice-distilled water. Hydrated slides were further rinsed in twice-distilled water using a shaker. Next, the slides were placed in Masson A solution and heated at 65 °C for 30 minutes, followed by overnight room temperature soaking. Thereafter, slides were rinsed in tap water. Next, Masson B and Masson C solutions were mixed, applied to the tissue sections, and incubated for 1.5 minutes, followed by rinsing with tap water. Color differentiation was performed using 1% hydrochloric acidalcohol solution for 3-5 seconds, followed by a 10-minute tap water rinse. Then, slides were

immersed in Masson D solution for 6 minutes, followed by thorough rinsing in tap water. Masson E solution was next applied for 1 minute. Without rinsing, slides were placed in Masson F solution for 30 seconds, followed by a tap water rinse. Next, slides were briefly dipped in 1% acetic acid for 2 seconds, then rinsed with tap water. Dehydration and clearing steps involved the sequential immersion in 80% ethanol, 95% ethanol, 100% ethanol I, 100% ethanol II, xylene I, and xylene II. Finally, the sections were mounted on slides using neutral gum, and any gum excess was carefully removed.

Results

1.Patients included in this clinical study

A total of 53 burnt patients (Table 4) were included in this study, of which 71.7% were male and 28.3% were female. The average values of patients' features are reported in Table 4.

Table 4. Patients and samples baseline values

Patients and samples	
Patients (n)	53
Age (mean ±SD)	38.27 ±14.98
Gender (male/female)	38/15
Height (mean ± SD)	1.61 ±0.17
Weight (mean ±SD)	62.82 ±16.08
BMI (mean ±SD)	23.66 ±3.43
Total wound samples (n)	171
Included wound samples (n)	76
Biopsy sites (n (%))	
Upper arm	15 (19.7)
Lower arm	20 (26.4)
Hand	7 (9.2)
Thigh	15 (19.7)
Lower leg	18 (23.7)
Foot	1 (1.3)

We collected 171 wound samples from all the patients mentioned above for spectral information collection and histopathological analysis. With the preliminary analysis of the data based on the first 23 patients with 34 wounds, we found that various interference factors related to spectral acquisition and pathological measurement may affect the application of spectral diagnosis. Therefore, we explored these factors (details in the Results following sections), by which the quality of the clinical study, particularly the stability of the spectral data obtained, could be better controlled. Finally, we successfully recruited 76 wound samples from 15 upper arms, 2 lower arms, 7 hands, 15 thighs, 18 lower legs, and 1 foot.

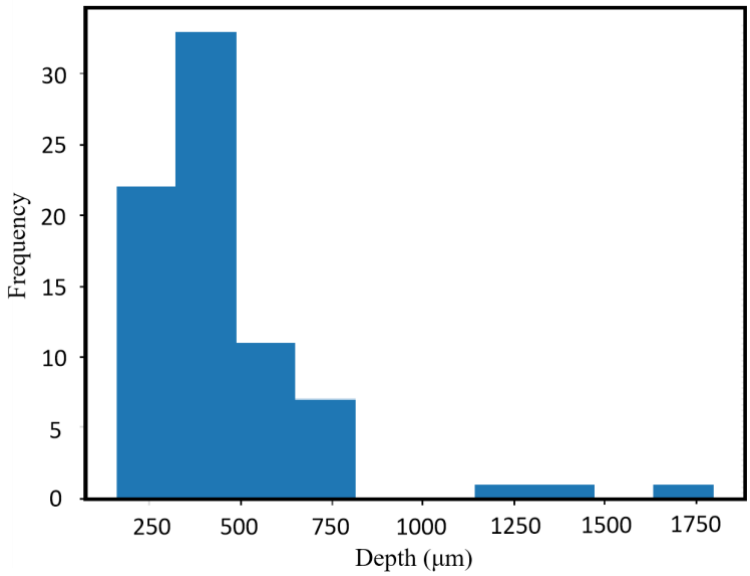

Figure 2. The histology measurement statistics of the included samples showed that the depth values of most burn samples were concentrated around 200-800um. The x-axis represents the necrotic depth (μ m) measured histologically for the wound, while the y-axis represents the number of wound samples in that depth range.

By calculating the depth values of the burn data, the histogram of depth distribution is shown in Figure 2. It can be seen that most of the burn depths are concentrated in the range of 200-800um, with the largest number of samples around 400μm. Therefore, a model trained with this data as a training set may have higher accuracy in predicting depths around 400μm when fitted to new data.

2.Factors impacting on spectral data stability

As wounds are overly complicated by the concurrence of exudate, uneven surfaces, locally applied medications, etc., which might affect the spectral data collection, several potential influence factors were evaluated at the beginning of this clinical study.

2.1 Wound Exudation

During the wound collection process, it was observed that some wounds will continue release exudates (Fig. 3a). As a result, the black and white spectral images captured by the near-infrared (NIR) showed an overexposure (Fig. 3b). To investigate this further, spectra were extracted from the same sample at both the exudate and non-exudate sites with similar pathological burn depths.

It could be seen that the presence of wound exudate was more likely to cause light reflection (Fig. 3a). From the NIR spectral imaging (Fig. 3b), it could be seen that the exudation was closer to the NIR light band, which could also cause many reflective points. At this position, the band's brightnesswas obviously higher. Compared with the wound position with no abnormal reflection, the spectral curve of the reflective position showed a high signal overall, and was not smooth, showing a considerable number of irregular peaks. Spectral curves were obtained from 10 pixels in each of the two areas (Fig. 3c). Significantly different spectral reflectance values were observed at wavelengths of 900 nm, 1000 nm, 1100 nm, 1200 nm, 1300 nm, 1400 nm, 1500 nm, and 1600 nm ($p < 0.01$) (Table 5).

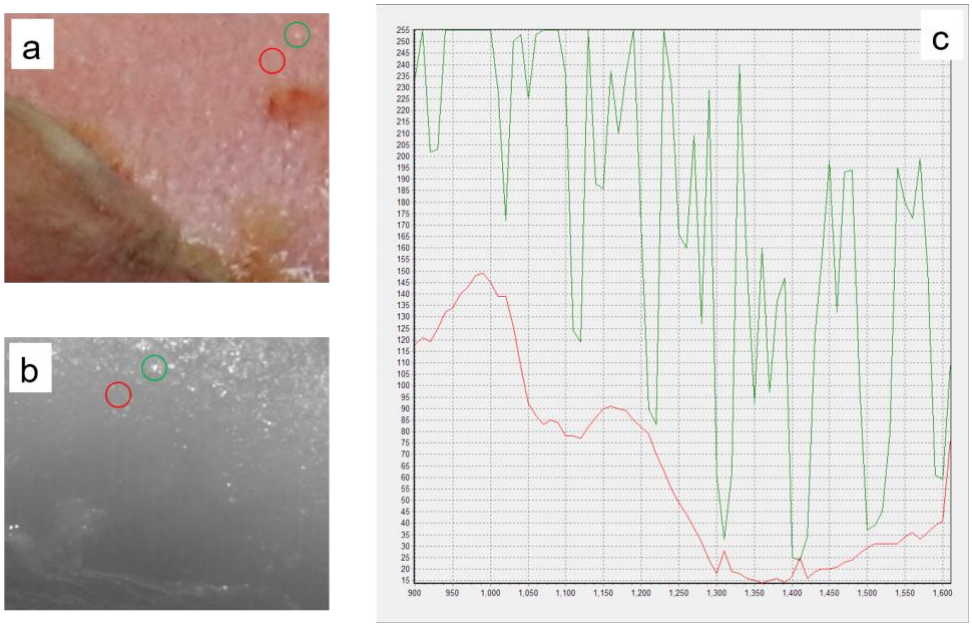

Figure 3. The influence of an exudating wound on the spectral curve morphology. (a) Photo of an exudating wound. (b) NIR spectral imaging of an exudating wound (the green circle is the highly reflective exudating area, while the red circle is the area devoid of any significant reflective exudate). Based on the shape of the skin contour, it could be determined that the areas circled in Figure 3a and Figure 3b are from the same site. (c) Spectral curves of exudating (green) and non-exudating (red) sites. Compared with the spectral curve of the non-exudative site (red curve), the spectral curve of the exudative site (green curve) had a very high average reflectance intensity, and the curve was not smooth, with a large number of peaks.

Table 5. Reflectivity at different wavelengths of non-exudating sites and of exudating sites.

	Reflectivity (mean (SD))		
	Non-exudating sites	Exudating sites	*p*
1000 nm	109.00 (1.00)	201.30 (28.27)	<0.01
1100 nm	59.20 (0.75)	113.70 (22.41)	<0.01
1200 nm	58.50 (0.67)	99.60 (11.39)	<0.01
1300 nm	12.50 (0.67)	32.10 (8.78)	<0.01
1400 nm	9.10 (0.54)	23.70 (4.90)	<0.01
1500 nm	15.90 (0.54)	37.30 (3.10)	<0.01
1600 nm	28.50 (2.46)	57.80 (4.94)	<0.01

2.2 Wound Shaking

During the collection of burn wound spectra using the novel spectral imaging device, a few patients experienced slight movements or jitters, leading to displacements of the target area. To assess the impact, spectral curves were extracted from 10-pixel points of samples affected by shaking and compared to static samples with consistent pathological burn depth.

During the spectral imaging of the wound, when the acquisition was performed at a wavelength of 1440 nm, the patient's limb experienced a large amplitude shaking. As shown in Figure 4, the target wound did not appear in the same position in the 1440 nm image as it did in the 1000 nm image. Once selecting the spectrum at the location of the red mark, the spectral curve suddenly appeared as a high signal peak at 1440 nm, while the curves in other bands remained smooth.

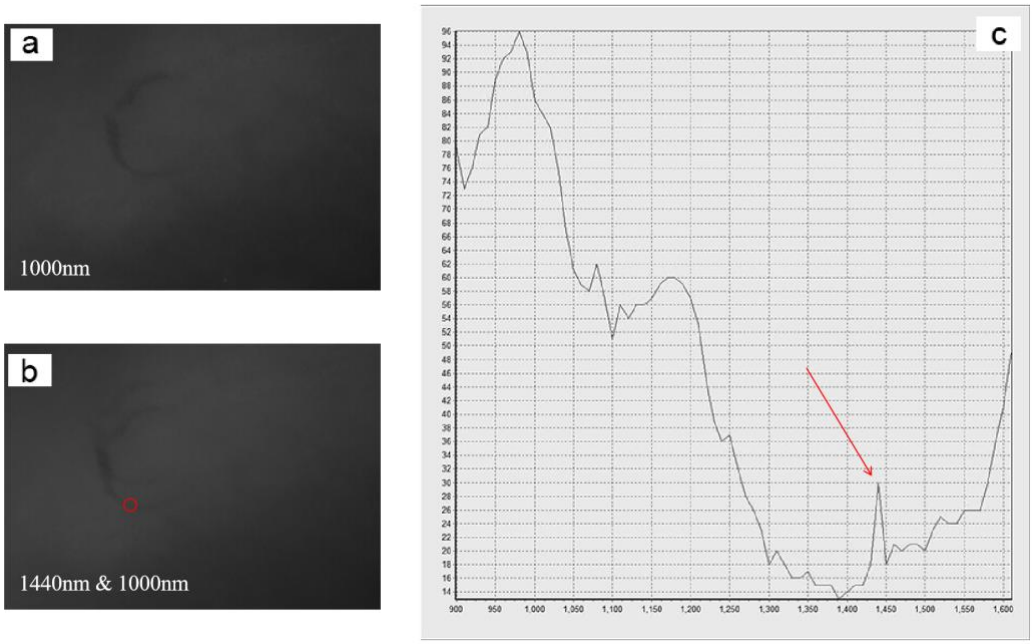

Figure 4. Spectral imaging and curves of a vibrating wound. (a) Non-vibrating wound NIR spectral imaging. The visible imaging appears more clear. (b) Vibrating wound NIR spectral imaging. Due to the vibrations that occurred during the imaging process at the 1440nm wavelength, the marked location appears visibly different from when imaged at 1000nm. (c) Obtained the spectral curve of the wound from the red circle in Figure 4b. The red arrow points to the 1440nm wavelength where a significant abnormal peak appears in the spectral curve.

2.3 Uneven tissue

Spectra were extracted from the same sample, comparing the part facing the SIT device to the part at a certain angle with the SIT device, both at the same burn depth. It could be seen that, in terms of curve details and reflection values in each band, the spectral curve of the same part when facing the camera differed from the spectral curve when it did not face the camera. Ten-pixel points were analyzed for each location. Significant differences in spectral reflectance values were observed at wavelengths 1000 nm (p = 0.02), 1100 nm, 1200 nm, 1300 nm, 1400 nm, 1500 nm and 1600 nm (p < 0.01). This might happen because, with necrotic tissues of the same thickness, , the t of necrotic tissue thickness appears to be deeper in the direction of the lens,when the latter faces sideways. .

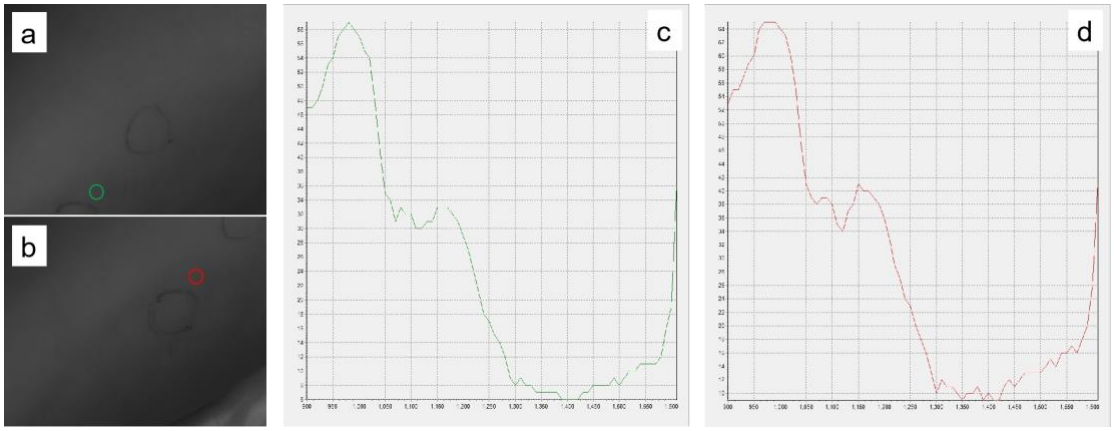

Figure 5. Spectral imaging results of the same site in two imaging positions. (a) Target spot at an angle to the SIT device. (b) Target spot facing the SIT device. The green and red circles next to the left marked site indicate the same location on the wound surface. (c) Spectral curves of the site in the green circle. (d) spectral curves of the site in the red circle. The two spectral curves exhibited similar shapes, but there were subtle differences in values, such as the fact that the green curve had a maximum reflection value of only 60, while the red curve had a maximum reflection value of 66.

Table 6. The reflectivity of wounds at different wavelengths and angles.

	Reflectivity (mean (SD))		
	Perpendicular	Forming an angle	*p*
1000 nm	64.40 (0.92)	63.20 (1.08)	0.02
1100 nm	36.50 (0.67)	35.20 (0.87)	<0.01
1200 nm	34.70 (0.64)	33.30 (0.64)	<0.01
1300 nm	11.40 (0.49)	9.10 (0.30)	<0.01
1400 nm	9.60 (0.80)	7.00 (0.45)	<0.01

1500 nm	13.30 (0.64)	10.80 (0.75)	<0.01
1600 nm	26.80 (1.47)	22.90 (1.22)	<0.01

2.4 Wound treatment

Microscopic observations of tissue specimens were sampled from around the tension reduction site revealed the presence of a full-thickness edema and a disordered collagen fibers arrangement. This picture significantly differed from the collagen degeneration observed in burnt tissues (Figure 6). Consequently, tissue spectral data from the tension reduction site were not included in the burn wound spectral database.

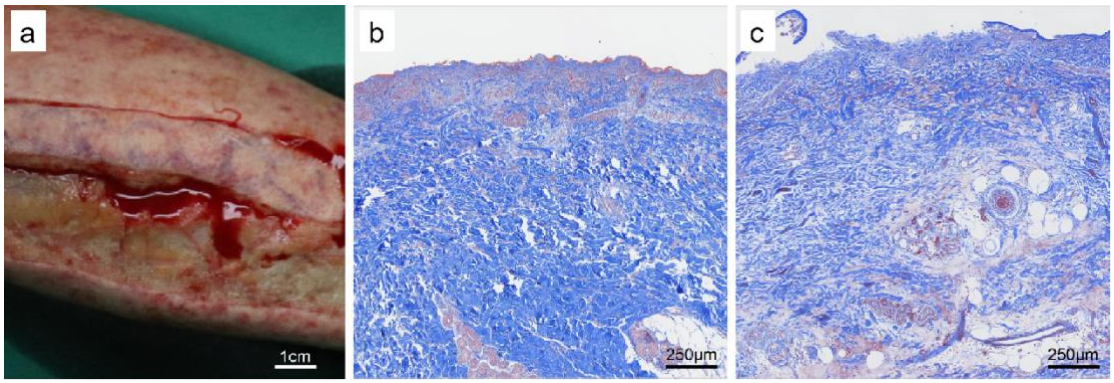

Figure 6. The effects of tension reduction. (a) Photo of incision site. After incision and tension reduction, local skin bleeding and more exudation were observed. (b) Pathological image of a non-tension reduction tissue area. The superficial layer of dermis showed abnormal red staining and structural loosening due to damage to collagen fibers, while the deepest layer of collagen fibers exhibited the same orderly arrangement and blue staining as normal skin. (c) Pathological image of a tension reduction tissue area. Due to edema, congestion, and other changes in the dermal tissue, the tissue structure of the entire skin layer became loose and red, masking the changes in collagen fibers caused by burn injury.

3.Raw spectral data

From September 2020 to January 2022, we collected a total of 23 patients , and numbered them according to their enrollment order from 01001 to 01023. From them we collected a total of 34 wound samples. Due to the uneven depth of the

necrosis in patient No. 01023's wound, we selected as test targets five sites in this wound (Fig. 7).

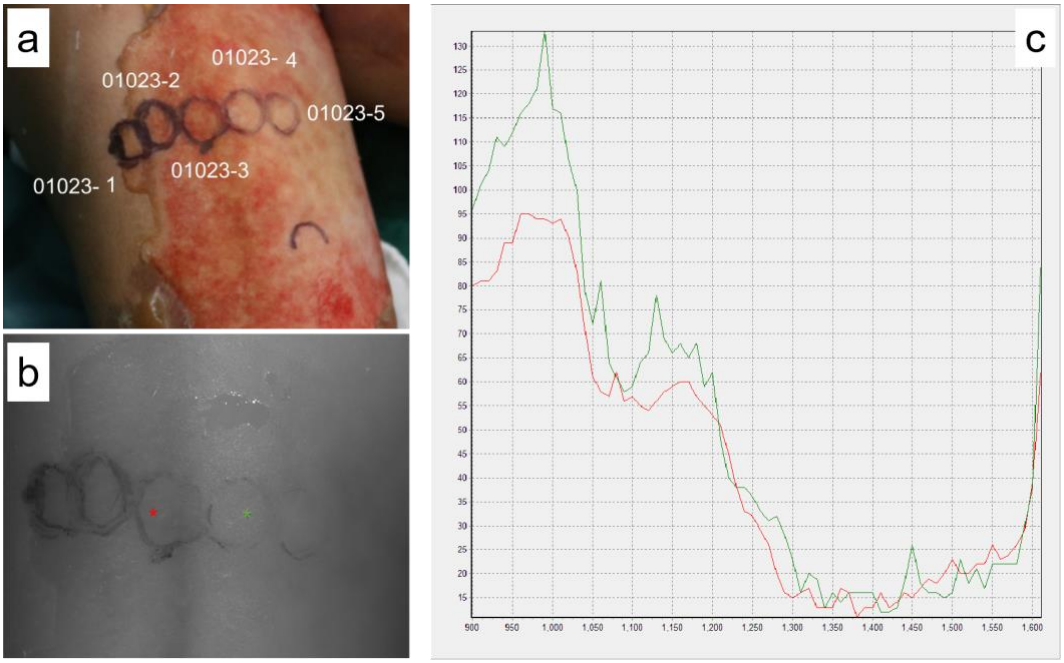

Figure 7. An example of No. 01023 patient's spectral curves. (a) Photograph of the wound on patient 01023's upper arm. According to clinical visual diagnosis methods, the uneven color of the wound surface indicates that the depth of burn necrosis in this wound is complex. (b) Spectral image at a wavelength of 1000 nm for the same wound on patient 01023 as in (a). (c) Raw spectral curves for the red and green marked points on the wound of patient 01023 as in (b). For wounds with different depths of necrosis, the shape of the spectral curve and the reflectance values of each wavelength band showed significant differences.

As just mentioned, five selected wound sites were located on the patient's upper arm. The wound base was red and white, which was consistent in clinical practice with the typical appearance of mixed second-degree burn wounds. It could be seen from the NIR imaging at 1000 nm (Fig. 7b) that the local reflectivity for this wavelength of the wound on the right side was lower, resulting in la less intense imaging brightness. Conversely, the left side exhibited a higher reflectivity, resulting in a more intense imaging brightness. Even from the raw (i.e. with no pre-processing) spectral curves it was clear that the curve on the right side had a lower intensity than that on the left side of the wound. The spectral curves of the wounds on both sides could be neatly distinguished in the 900-1700 nm wavelength range,

proving that medical near-infrared spectrometers could differentiate wounds with different burn intensity degrees.

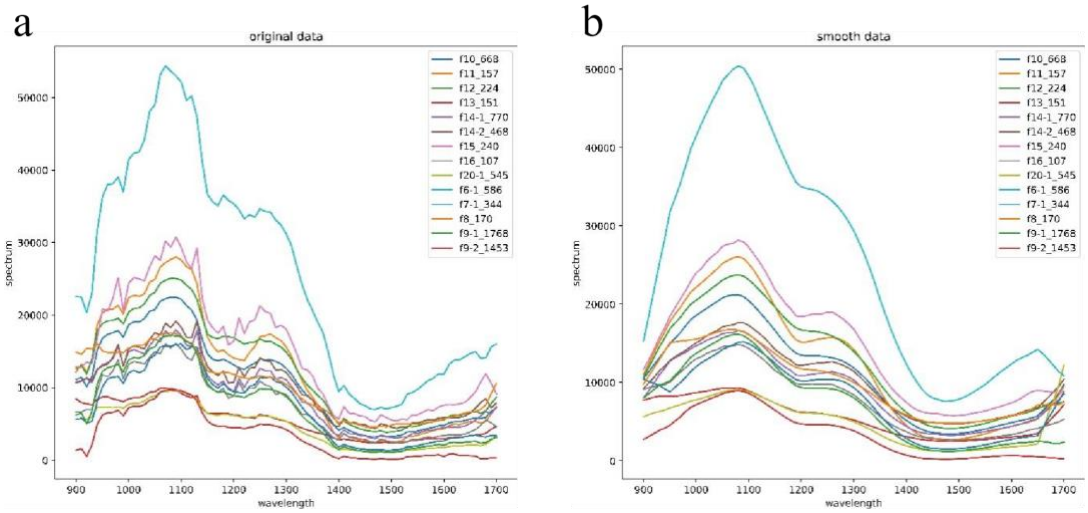

Figure 8. Spectral curves pre-processing. (a) Before pre-processing, there were many small peaks in the raw spectral curve, which partially obscured the differences in spectral curves between different wound. (b) After pre-processing, it could be seen that the spectral curve shape and value were different for wounds with different burn depth.

The spectral curves of wounds with different burn necrosis depths (Fig. 8) were more easily distinguished after pre-processing such as filtering. After preliminary normalization and smoothing filtering, a smooth spectral curve could be obtained. It could be seen that wounds with different burn necrosis depths have significant differences in their spectral curves, with greater differences in the wavelength range of 900-1400nm.

4. Optimizing the burn depth regression model using principal component analysis

Using data with a wavelength range of 900-1700nm (full-spectrum), principal component analysis (PCA) was applied for dimensionality reduction, retaining 99% of the principal components to eliminate a small amount of noise points. The mean absolute percentage error (MAPE) was employed as an evaluation metric. Input the

entire image of samples into the model and draw a pseudo-color map based on the prediction results. The results are shown in Figure 9:

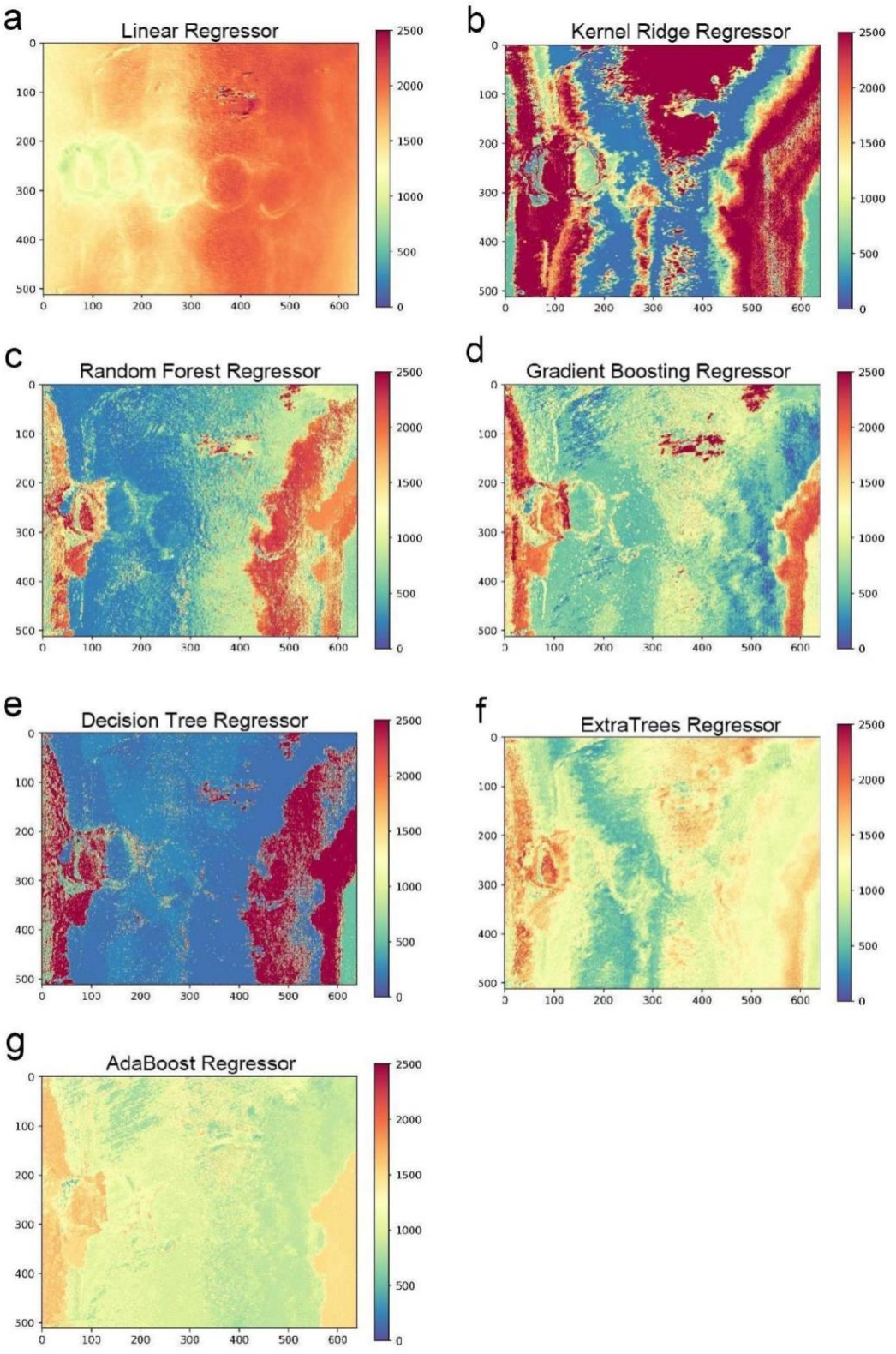

Figure 9. Pseudo-color maps of different regression models. (a) Linear Regression, (b) Kernel Ridge Regression, (c) Random Forest Regression, (d) Gradient Boosting Regression, (e) Decision Tree Regression, (f) Extra Trees Regression, and (g) AdaBoost Regression. The numbers on the edge of each image were used as a positional reference, and the stripes on the right indicated different colors representing the corresponding necrosis depth, with the unit being μm.

After applying PCA for dimensionality reduction of the spectral information, the noise points in the pseudo-color maps reconstructed from the prediction values were reduced to a certain extent (Fig. 9). It could be seen that the pseudo-color maps reconstructed based on models such as Linear Regression, Kernel Ridge Regression, Random Forest Regression, Gradient Boosting Regression, Decision Tree Regression, Extra Trees Regression, etc. all had large areas of predictions with depths greater than 1500 μm, which was significantly inconsistent with our histological measurement (Fig. 2). The depth values predicted by the Adaboost regression model were consistent with our histological measurement results and could generate smoother pseudo-color maps.

Although the average prediction error for some wound surfaces was only about 20% after pre-processing the spectral data and applying PCA for dimensionality reduction, there was still a need for new training samples to increase the robustness of the model.

5.Increase sample size

Based on the pre-experiment, the PCA+Adaboost model had the least amount of false color images generated from fitting the test set and had a small error rate. Therefore, after using PCA to reduce the dimension of the data, we selected the PCA+Adaboost model for modeling. The following figure is a fitting graph of the patient's burn depth. As shown in Figure 10, the burn depth trend predicted by this experiment is consistent with the actual situation, but the overall depth value prediction is lower than the true value.

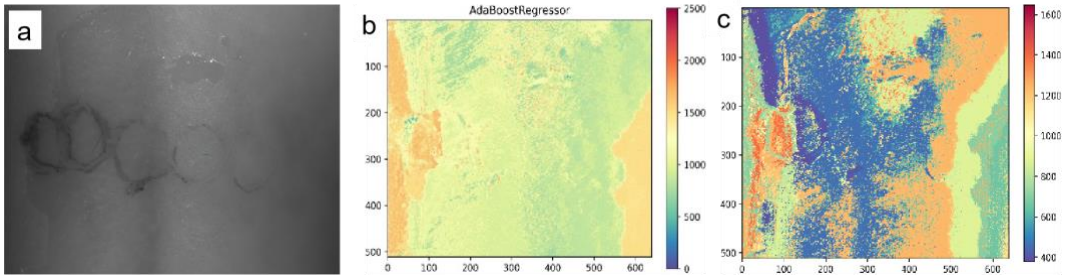

Figure 10. The fitting effect of the PCA+Adaboost model on the depth of burns in patients. (a) The original burn spectral imaging map. (b) The fitting map of the depth of burns in a small amount of data showed that the predicted depth was generally within the range of the histological detection results, but the internal details displayed for this uneven necrotic wound were still not rich enough. (c) The fitting map of the depth of burns in the data after increasing the sample size showed that the prediction range remained accurate, while the details had been significantly enriched. The numbers on the edge of each pseudo-color maps were used as a positional reference, and the stripes on the right indicated different colors representing the corresponding necrosis depth, with the unit being μ m.

Selected part of the wound's full-band data as the training set, the remaining part as the full-band data as the test set, using the average absolute percentage error (MAPE) as the evaluation index, established an AdaBoost regression model to predict the patient data. Considering the randomness of the model, each experiment was run 10 times, and the standard deviations of the prediction results were calculated. The experimental results were shown in the table 7.

Table 7. Prediction Results of Wound Data in Test Set.

Sample	Real depth(μm)	Predicted depth(μm)	MAPE (%)
01006-1	517	512.67±9.80	0.83
01012	366	404.03±9.80	10.29
01014-2	396	410.96±24.80	5.45
01024	428	409.02±21.60	6.37
01029-1	306	382.16±28.74	24.62
01030-3	450	444.31±19.34	2.61
01035-1	297	316.38±56.02	9.30
01039-4	378	432.84±29.33	14.88
01039-7	447	414.90±35.94	8.01
01040-3	422	399.38±32.29	7.42
01042-1	641	403.06±5.35	37.11
01036-2	677	410.82±27.90	39.34
01037-3	806	489.03±29.37	39.37

01037-6	737	423.20±33.77	42.60

As shown in table 7, the standard deviation of the model prediction results was mostly below 50 μm, indicating that the model had a certain stability. For samples with a burn depth of 100μm-200μm, such as sample 01043-1 with a true burn depth of 159μm, the predicted result is 418.11±34.92μm with a MAPE of 162.41%, indicating a larger prediction bias for shallower depth values. For samples with a burn depth of 200μm-700μm, such as sample 01006-1 with a true burn depth of 517μm, the predicted result was 512.67±9.80μm with a MAPE of 0.83%, indicating more accurate predictions for this range of burn depths. For samples with a burn depth of 700μm-800μm, such as sample 01037-3 with a true burn depth of 806μm, the predicted result was 489.03±29.37 MAPE with a MAPE of 39.37%, indicating a prediction bias for this range of burn depths.

Machine learning was data-driven and heavily relies on the training dataset, which consisted of high-quality data with burn depth values concentrated within the range of 300-700 μm. Therefore, models trained with this data had relatively accurate predictions for test samples within this range. Subsequent work could include increasing the number of samples in the 100-200 μm and 700-800 μm depth ranges to improve the model's accuracy for predicting samples within these ranges.

Discussion

1. Significance

Currently, objective measurement of burn wound depth remains a challenging, presenting a significant conundrum in burn wound management. Accurately ascertaining wound depth is of paramount importance in providing tailored care for burn patients, optimizing their treatment plans, and enhancing therapeutic outcomes. Within this context, a pressing scientific inquiry has arisen: can an imaging technology be developed to precisely diagnose the depth of necrotic tissue in burn wounds, thereby bridging crucial diagnostic gaps and offering a more effective approach to burn wound treatment? Addressing this question not only

resolves immediate clinical needs but also holds the potential to transform the landscape of wound precision diagnosis and treatment.

Drawing on the principles of near-infrared spectroscopy, a promising avenue has emerged to confront the challenge of accurately measuring wound depth. The interaction of near-infrared light with tissue produces a spectrum that contains absorbance, reflectance, or transmittance data over a range of near-infrared wavelengths. This spectrum reflects the unique optical properties of the tissue and is affected by the tissue's composition and structure. For example, hemoglobin absorbs near-infrared light differently when it is oxygenated or deoxygenated, providing information about blood flow and oxygenation. Near-infrared spectroscopy assesses the interaction between near-infrared light and tissues, opening the door to precise measurement of the depth of necrotic tissue within wounds. This technology not only provides a non-invasive means to evaluate tissue characteristics but also unlocks new possibilities for the accurate measurement of wound depth, a long-standing but elusive goal within the field of medical diagnostics.

In recent years, our research team has undertaken a series of experiments, encompassing in vitro skin samples and in vivo animal models, to explore the feasibility, sensitivity, and initial parameter selection for near-infrared spectroscopy imaging technology.

Our exploration commenced with an analysis of tissue composition information within the near-infrared diffuse reflectance spectrum of isolated porcine skin, including hemoglobin levels and water content, as well as structural data pertaining to particle size and particle density. Through rigorous training, we constructed an inversion model based on support vector machine learning, successfully enabling the evaluation of burn depth in ex vivo porcine skin. Impressively, the overall average relative error of the model's detection was as low as 7.63%, providing robust evidence for the feasibility of near-infrared spectroscopy technology in burn wound diagnostics. Subsequently, we conducted in vivo animal experiments.

We observed a significant correlation between the scattering particle density parameter and burn depth in these live animal experiments. However, parameters

such as water content and particle size did not exhibit significant correlations with burn depth. This observation can be attributed to the dynamic physiological and pathological changes in live animals, including congestion and edema, which introduced additional variables into burn depth prediction.

Recognizing the complexity of in vivo burn wounds, we turned to transfer learning techniques to address the challenges posed by diverse influencing factors. By developing a convolutional neural network (CNN) prediction model for transfer learning, we achieved remarkable accuracy. The maximum difference between the average depth value predicted by this model for the validation set and the actual depth value was only 32 μm, demonstrating the robustness and precision of our approach.

These results provide compelling evidence of the potential of near-infrared spectroscopy to accurately measure burn wounds. Our next critical step will be to validate the feasibility and accuracy of this technology in human burn wounds.

To fulfill our experimental goals, we designed our clinical study. Firstly, we maintained the highest accuracy standards by using histological values from tissue biopsy as the benchmark for data training. Secondly, we conducted a secondary screening of collected samples to identify and eliminate factors that could compromise the quality of spectral data. This process not only ensured the robustness of our data but also provided valuable insights for improving our sample collection protocols and enhancing spectral quality in subsequent experiments. Finally, recognizing the inherent differences between animal wounds generated under controlled laboratory conditions and clinical patient wounds, we reevaluated our modeling methods. This step enabled us to identify the most suitable approach for clinical wound detection, making our technology adaptable to the complexities of real-world scenarios.

Finally, the PCA-based Adaboost regression model emerged as the most effective model, demonstrating an elevated level of prediction accuracy. It is important to note that within the necrotic tissue depth range of 200 μm to 600 μm, this model exhibited significant accuracy and stability, with a standard deviation of less than 50 μm.

However, it must be acknowledged that this model has limitations in predicting burn depths below 200 μm or above 600 μm. We could not understand very well why the very superficial burn wounds could not be precisely assessed; further study is needed. While, for deeper wounds, a range of factors, such as fluid exudation, motion artifacts, surface irregularities, incision variations and tension alterations participated in influencing model accuracy. These multifaceted considerations underscore the complexity of predicting burn wound depth and guide future research endeavors.

2. Comparison with Existing Methods

While various modern technologies for burn depth diagnosis, including spectroscopy, have been reported, they often classify burn wounds into different degrees [45,46]. Among these, Laser Doppler Imaging (LDI) is the sole FDA-approved device for assessing burn wound depth. LDI distinguishes burn depth based on differences in blood flow velocity across burn wounds. Nevertheless, LDI indirectly assesses the extent of burn wound damage by measuring tissue perfusion and cannot directly measure the depth of necrotic tissue.

The results of our clinical study affirm that the burn necrotic tissue depth diagnosis model we developed could be a very promising objective approach that is difference from the traditional 3-degree dichotomy for burn severity evaluation. This novel approach achieved the goal of micron-level quantitative diagnosis, ushering in a new era of precision wound assessment.

In conclusion, the study highlights the potential of near-infrared spectroscopy imaging technology to accurately determine burn wound depth. However, to meet the demand for intelligent and accurate diagnosis, there is a need to increase the volume of wound spectrum data in clinical research, improve the accuracy of the prediction model, and realize precise clinical diagnosis of burn wound necrosis depth in patients.

Near-infrared spectroscopy offers a myriad of advantages that make it an indispensable tool in the field of medical diagnostics. Primarily, its efficiency and speed are commendable, as it obviates the need for sample processing and swiftly completes the detection process in as little as one minute [47]. Such expeditious data

acquisition is especially critical in the context of burn wound assessment, where timely information is of paramount importance. Another notable advantage is its exceptional penetration depth. Near-infrared photons are minimally affected by water signals, allowing them to penetrate living tissue to depths ranging from 5 to 10 mm [48]. This deep tissue penetration proves invaluable in accurately gauging the extent of burn injuries. Furthermore, the technology is marked by its safety and non-invasiveness. Operating within the harmless near-infrared band of the natural spectrum, it poses no risk to human health, distinguishing it from methods involving contrast agents like indocyanine green (ICG) dye [49]. In addition, it boasts an inherent infection control advantage. Unlike techniques such as orthogonal polarization spectroscopy, which necessitate direct contact with the wound, non-contact NIR diagnostics minimize the risk of cross-contamination—a critical consideration in clinical settings [50]. The objectivity of results is another defining feature, with near-infrared spectroscopy rendering diagnostic outcomes that do not depend on physician expertise or operator subjectivity. This objectivity ensures the reliability of results, free from interpretive artifacts, as well as is critical for future precision debridement.

Moreover, near-infrared spectral information contains a wealth of data about the sample, offering potential for the development of detection systems for various clinical indicators. This expansion can significantly impact the domains of clinical diagnostics, cell biology, and related disciplines. Finally, with the advancement of artificial intelligence and related fields, the integration of near-infrared spectrometers with precise tissue debridement equipment has the potential to revolutionize the landscape of diagnosis and treatment, promoting a holistic and integrated approach to patient care.

The above mentioned advantages underscore the exceptional capability of medical near-infrared spectrometers in distinguishing the degree of wound necrosis. However, to meet the growing demand for intelligent and accurate diagnosis, it is imperative to accumulate a larger volume of wound spectrum data in clinical research. This expansion will enhance the accuracy of prediction models, culminating in the precise clinical diagnosis of the depth of necrosis in patients' burn wounds.

3. Limitations

Despite the promising outcomes of our study, several limitations have come to our attention, necessitating acknowledgment and further exploration in future research. A substantial challenge in clinical study is the potential interference stemming from various physiological and non-physiological factors during the measurement process. Factors such as age, gender, collection location, body temperature, metabolism, blood flow, as well as instrument and environmental variables, collectively impact the collection of spectral signals. This intricate web of variables complicates the precise quantification of absolute spectral signals.

In the pursuit of improved stability and accuracy within diagnostic models, we advocate for a multifaceted approach. Firstly, we propose the implementation of more rigorous and expansive studies to establish normative data. This endeavor encompasses the definition of standardized operating procedures and the accumulation of substantial quantities of high-quality spectroscopic data. Increasing the number and quality of samples is aimed at reducing the impact of interference factors and improving prediction accuracy.

Secondly, we recognize the need for algorithmic enhancements to diminish the impact of these multifarious factors. The development of chemometric methods assumes paramount importance in addressing the intricacies of spectral bands and the diverse compositions of human tissue. These methods are pivotal in crafting resilient calibration models, replete with robust predictive capabilities for each detection indicator [51].

Lastly, by fostering integration among diverse data sources, near-infrared spectroscopy can be harmonized with other monitoring equipment, fostering comprehensive analysis and evaluation. This synergistic approach holds the promise of enhancing the model's accuracy and bolstering its reliability, paving the way for more dependable diagnostic outcomes.

Conclusions

Our study is a pioneering endeavor that utilizes near-infrared spectrum imaging technology in conjunction with intelligent data analysis to non-invasively acquire and visually quantify skin necrotic tissue depth information. This innovative approach not only equips future clinicians with an objective reference for precise burn depth diagnosis but also forms the cornerstone for advancing wound healing, reducing hypertrophic scar formation, and ushering in the era of intelligent and precise debridement. Our research's profound implications extend to the realms of clinical practice and regenerative medicine, offering a transformative paradigm for wound diagnosis and treatment.

Acknowledgments

The author would like to express his heartfelt gratitude to the following individuals whose unwavering support and contributions were instrumental in the successful completion of this research project:

Dr. Yin Meifang and Dr. Yuan Mingzhou, for their invaluable guidance and support in experimental design.

Professor Ubaldo Armato, for his invaluable aid during the writing process of this thesis.

Zhang Dayong and Luo Yongquan, for their technical ability and support in improving our equipment.

Wei Yating and Yuan Mingzhou, for their dedicated efforts in collecting clinical study data.

References

1.Kuwatsuka Y, Murota H. Involvement of Periostin in Skin Function, and the Pathogenesis of Skin Diseases[J]. Adv Exp Med Biol,2019,1132:89-98.

2.Tompkins R G, Burke J F, Schoenfeld D A, et al. Prompt eschar excision: a treatment system contributing to reduced burn mortality. A statistical evaluation of burn care at the Massachusetts General Hospital (1974-1984) [J]. Ann Surg,1986,204(3):272-281.

3.Kao CC, Garner WL. Acute Burns. Plast Reconstr Surg. 2000 Jun;101(7):2482-2493.
4.Monstrey S, Hoeksema H, Verbelen J, et al. Assessment of burn depth and burn wound healing potential[J]. Burns,2008,34(6):761-769.
5.Yoshino Y, Ohtsuka M, Kawaguchi M, et al. The wound/burn guidelines - 6: Guidelines for the management of burns[J]. J Dermatol,2016,43(9):989-1010.
6.Heimbach DM, Afromowitz MA, Engrav LH, Marvin JA, Perry B. Burn depth estimation--man or machine. J Trauma. 1984 May;24(5):373-8.
7.Niazi ZB, Essex TJ, Papini R, Scott D, McLean NR, et al. New laser Doppler scanner, a valuable adjunct in burn depth assessment. Burns 19: 485-489.
8.Ong Y S, Samuel M, Song C. Meta-analysis of early excision of burns. Burns,2006,32(2):145-150.
9.Piotrowski J, Anisimowicz L, Hellmann M. Laser Doppler flowmetry to assess myocardial microcirculation[J]. Cardiol J,2020.
10.Tang G L, Kim K J. Laser Doppler Perfusion Imaging in the Mouse Hindlimb[J]. J Vis Exp,2021(170).
11.Wang R, Zhao J, Zhang Z, et al. Diagnostic Accuracy of Laser Doppler Imaging for the Assessment of Burn Depth: A Meta-analysis and Systematic Review[J]. Journal of burn care & research,2020,41(3):619-625.
12.Gioux S, Mazhar A, Cuccia D J. Spatial frequency domain imaging in 2019: principles, applications, and perspectives[J]. J Biomed Opt,2019,24(7):1-18.
13.Mazhar A, Saggese S, Pollins A C, et al. Noncontact imaging of burn depth and extent in a porcine model using spatial frequency domain imaging[J]. J Biomed Opt,2014,19(8):86019.
14. Du E, Shen S, Chong S P, et al. Multifunctional laser speckle imaging[J]. Biomed Opt Express,2020,11(4):2007-2016.
15. Zieger M, Kaatz M, Springer S, et al. Multi-wavelength, handheld laser speckle imaging for skin evaluation[J]. Skin Res Technol,2021,27(4):486-493.
16. Zheng K J, Middelkoop E, Stoop M, et al. Validity of laser speckle contrast imaging for the prediction of burn wound healing potential[J]. Burns,2021.
17. Lu J, Deegan A J, Cheng Y, et al. Application of OCT-Derived Attenuation Coefficient in Acute Burn-Damaged Skin[J]. Lasers in Surgery and Medicine,2021,53(9):1192-1200.
18. Podoleanu A G. Optical coherence tomography[J]. J Microsc,2012,247(3):209-219.
19. Deegan A J, Mandell S P, Wang R K. Optical coherence tomography correlates multiple measures of tissue damage following acute burn injury[J]. Quantitative Imaging in Medicine and Surgery,2019,9(5):731-741.

20. Psomadakis C E, Marghoob N, Bleicher B, et al. Optical coherence tomography[J]. Clin Dermatol,2021,39(4):624-634.
21. Medina-Preciado J D, Kolosovas-Machuca E S, Velez-Gomez E, et al. Noninvasive determination of burn depth in children by digital infrared thermal imaging[J]. J Biomed Opt,2013,18(6):61204.
22. Ring E F, Ammer K. Infrared thermal imaging in medicine[J]. Physiol Meas,2012,33(3): R33-R46.
23. Mcumber H, Dabek R J, Bojovic B, et al. Burn Depth Analysis Using Indocyanine Green Fluorescence: A Review[J]. Journal of Burn Care & Research,2019,40(4):513-516.
24. Reinhart M B, Huntington C R, Blair L J, et al. Indocyanine Green: Historical Context, Current Applications, and Future Considerations[J]. Surg Innov,2016,23(2):166-175.
25. Wongkietkachorn A, Surakunprapha P, Jenwitheesuk K, et al. Indocyanine Green Angiography Precise Marking for Indeterminate Burn Excision: A Prospective, Multi-centered, Double-blinded Study[J]. Plastic and Reconstructive Surgery - Global Open,2021,9(4): e3538.
26. Lin Y, Huang C, Wang S. Quantitative assessments of burn degree by high-frequency ultrasonic backscattering and statistical model[J]. Physics in Medicine and Biology,2011,56(3):757-773.
27. Jiang X, Li F, Chi Y, et al. Application of contrast-enhanced ultrasound in the diagnosis of burn depth[J]. Ann Transl Med,2021,9(16):1315.
28. Lee S, Rahul, Ye H, et al. Real-time Burn Classification using Ultrasound Imaging[J]. Sci Rep,2020,10(1):5829.
29. Park S, Jang J, Kim J, et al. Real-time Triple-modal Photoacoustic, Ultrasound, and Magnetic Resonance Fusion Imaging of Humans[J]. IEEE Transactions on Medical Imaging,2017,36(9):1912-1921.
30. Amini T, Jahangiri F, Ameri Z, et al. A Review of Feasible Applications of THz Waves in Medical Diagnostics and Treatments[J]. J Lasers Med Sci,2021,12: e92.
31. Dutta M, Bhalla A S, Guo R. THz Imaging of Skin Burn: Seeing the Unseen—An Overview[J]. Advances in Wound Care,2016,5(8):338-348.
32. Dutta M, Bhalla A S, Guo R. THz Imaging of Skin Burn: Seeing the Unseen-An Overview[J]. Adv Wound Care (New Rochelle),2016,5(8):338-348.
33.Richard M. Levenson, MD. Spectral Imaging and Pathology: Seeing More. Laboratory Medicine, Volume 35, Issue 4, April 2004, Pages 244–251.

34. Kohzo Homma, Hirokimi Shingu, Hiromichi Yamamoto, et, al. Application of an imaging s pectropolarimeterto agro-environmental sciences. Sensors, Systems, and Next-Generation Satellites VII, Proceedings of SPIE Vol. 5234, 2004, Pages 638-647.

35.H. Kurosaki, H. Koshiishi, T. Suzuki and K. Tsuchiya. Development of tunable imaging spectro-polarimeter for remote sensing. Advances in Space Research. Volume 32, Issue 11, December 2003, Pages 2141-2146.

36.Yuval Garini, Ian T. Young, and George McNamara. Spectral Imaging: Principles and Applications. 2006 International Society for Analytical Cytology. 735-747.

37. Werner Eisenbeiû, Jo Èrg Marotz, Jens-Peter Schrade. Refection-optical multispectral imaging method for objective determination of burn depth. Burns. 1999 Dec; 25:693-704.

38. Herke Jan Noordmans, Rowland de Roode, Rudolf Verdaasdonk. Compact multi-spectral imaging System for dermatology and neurosurgery. Medical Imaging 2007: Physics of Medical Imaging, Proc. of SPIE Vol. 6510.2007.

39. Rowland de Roode, Herke Jan Noordmans, Rudolf Verdaasdonk. Feasibility of multi-spectral imaging system to provide enhanced demarcation for skin tumor resection. Photonic Therapeutics and Diagnostics III, Proc. of SPIE Vol. 6424.2007.

40. Tuan Vo-Dinh, Paul Kasili and Brian Cullum. Multi-spectral Imaging for Medical Diagnostics Biomedical Diagnostic, Guidance, and Surgical- Assist Systems IV, Proceedings of SPIE Vol. 4615.2002.

41. Meifang Yin, Jiangfeng Li, Lixian Huang, et al. Identification of microbes in wounds using near-infrared spectroscopy. Burns. 2022 Jun;48(4):791-798.

42. Meifang Yin, Yongming Li, Yongquan Luo, et al. A novel method for objectively, rapidly, and accurately evaluating burn depth via near infrared spectroscopy. Burns Trauma. 2021 Jul; 9:9: tkab014.

43.Pin Wang, Yao Cao, Meifang Yin, et al. Full-field burn depth detection based on near-infrared hyperspectral imaging and ensemble regression. Rev Sci Instrum. 2019 Jun;90(6):064103.

44. Pin Wang, Yao Cao, Meifang Yin, et al. A burn depth detection system based on near infrared spectroscopy and ensemble learning. Rev Sci Instrum. 2017 Nov;88(11):114302.

45. Md Anowar Parvez, Kazuhiro Yashiro, Yasuyuki Tsunoi, et al. In vivo monitoring of hemoglobin derivatives in a rat thermal injury model using spectral diffuse reflectance imaging. Burns. 2023 Jul 26: S0305-4179(23)00140-7.
46.Zhiwei Li, Jie Huang, Xirui Tong, et al. GL-Fusionnet: Fusing global and local features to classify deep and superficial partial thickness. Burn. 2023 Mar 29;20(6):10153-10173.
47. Lin Y, Huang C, Wang S. Quantitative assessments of burn degree by high-frequency ultrasonic backscattering and statistical model. Phys Med Biol. 2011; 56:757–73.
48. Kim NS, Jin HY, Kim EY, Hong TH. Cystic duct variation detected by near-infrared fluorescent cholangiography during laparoscopic cholecystectomy. Ann Surg Treat Res. 2017; 92:47.
49. McUmber H, Dabek RJ, Bojovic B, Driscoll DN. Burn depth analysis using indocyanine green fluorescence: a review. J Burn Care Res. 2019; 40:513–6.
50. Goertz O, Ring A, Köhlinger A, Daigeler A, Andree C, Steinau H, et al. Orthogonal polarization spectral imaging. Ann Plas Surg. 2010; 64:217–21.
51.Mihaela Antonina Calin, Radu Robert Piticescu, Sorin Viorel Parasca, et al. Comparative analysis of denoising techniques in burn depth discrimination from burn hyperspectral images. J Biophotonics. 2023 Jul;16(7): e202200374.

Appendices

1. Scientific Publications

1. Wang X, Xu K, Mu L, Zhang X, Huang G, Xing M, Li Z, **Wu J**. Mussel-Derived Bioadaptive Artificial Tendon Facilitates the Cell Proliferation and Tenogenesis to Promote Tendon Functional Reconstruction. Adv Healthc Mater. 2023 Sep;12(24): e2203400. doi: 10.1002/adhm.202203400. Epub 2023 Jul 27. PMID: 37462927.

2. Yang G, Waheed S, Wang C, Shekh M, Li Z, **Wu J**. Exosomes and Their Bioengineering Strategies in the Cutaneous Wound Healing and Related Complications: Current Knowledge and Future Perspectives. Int J Biol Sci. 2023 Feb 27;19(5):1430-1454. doi: 10.7150/ijbs.80430. PMID: 37056923; PMCID: PMC10086759.

3. Wei Y, **Wu J**, Chen Y, Fan K, Yu X, Li X, Zhao Y, Li Y, Lv G, Song G, Rong X, Lin C, Wang H, Chen X, Zhang P, Han C, Zu H, Liu W, Zhang Y, Liu C, Su Y, Zhang B, Sun B, Wang L, Lai W, Liu J, Xia C, Ji G, Zhu F, Yu J, Ahemaiti A, Dong H, Chen M; PL-5 Investigators. Efficacy and Safety of PL-5 (Peceleganan) Spray for Wound Infections: A Phase IIb Randomized Clinical Trial. Ann Surg. 2022 Jul 4;277(1):43–9.

4. Wang M, Yao S, He D, Qahar M, He J, Yin M, **Wu J**, Yang G. Type 2 Diabetic Mellitus Inhibits Skin Renewal through Inhibiting WNT-Dependent Lgr5+ Hair Follicle Stem Cell Activation in C57BL/6 Mice. J Diabetes Res. 2022 Apr 16; 2022:8938276.

5. Wei Y, Li J, Huang Y, Lei X, Zhang L, Yin M, Deng J, Wang X, Fu X, **Wu J**. The clinical effectiveness and safety of using epidermal growth factor, fibroblast growth factor and granulocyte-macrophage colony stimulating factor as therapeutics in acute skin wound healing: a systematic review and meta-analysis. Burns Trauma. 2022 Mar 7;10: tkac002.

6. Wei Y, Li J, Huang Y, Lei X, Zhang L, Yin M, Deng J, Wang X, Fu X, **Wu J**. The clinical effectiveness and safety of using epidermal growth factor, fibroblast growth factor and granulocyte-macrophage colony stimulating factor as therapeutics in acute skin wound healing: a systematic review and meta-analysis. Burns Trauma. 2022 Mar 7;10: tkac002.

7. Hu P, Chiarini A, **Wu J**, Wei Z, Armato U, Dal Prà I. Adult human vascular smooth muscle cells on 3d silk fibroin nonwovens release exosomes enriched in angiogenic and growth-promoting factors. Polymers (Basel). 2022 Feb 11;14(4):697. doi: 10.3390/polym14040697. PMID: 35215609; PMCID: PMC8875541.

8. Yin M, Yuan M, Deng K, Li J, Zhang G, Zhu J, Xie W, **Wu J**. Subcutaneous Low-Density Foreign Bodies Detection via Grating-Based Multimodal X-ray Imaging. J Digit Imaging. 2022 Apr;35(2):365-373. doi: 10.1007/s10278-021-00569-5. Epub 2022 Jan 21. PMID: 35064371.

9. Meifang Yin, Lixian Huang, Yongming Li, Mingzhou Yuan, Yongquan Luo, Ubaldo Armato, Lijun Zhang, Dayong Zhang, Yating Wei, Yuanyuan Li, Jiawen Den, Pin Wang, **Jun Wu**. Identification of microbes in wounds via Near-Infrared Spectroscopy. Burns. Available online 17 September 2021

10. Meifang Yin, Yongming Li, Yongquan Luo, Mingzhou Yuan, Ubaldo Armato, Ilaria Dal Pra, Lijun Zhang, Dayong Zhang, Yating Wei, Guang Yang, Lixian Huang, Pin Wang, **Jun Wu**. A novel method objectively, rapidly, and accurately evaluating burns depth via near infrared spectropscopy. Burns & Trauma 2021;9: tkab014.

11. Yating Wei, Cecilia W P Li-Tsang, **Jun Wu**, Walei Zhang, Yingying Zhang, Huan Deng, Ming Zhang, Yan Wang. A finite element model of the 3D-printed transparent facemask for applying pressure therapy. Clinical Biomechanics 2021, 87:105414

12. Meishu Zhu, Meihui Zhu, Xiaoling Wu, Meiquan Xu, Kunwu Fan, Jinming Wang, Liyong Zhang, Meifang Yin, **Jun Wu**, Zhixiang Zhu, Guang Yang. Porcine

Acellular Dermal Matrix Increases Fat Survival Rate after Fat Grafting in Nude Mice. Aesth Plast Surg 2021 45:2426-2436

13. Pin Wang, Pufei Li, Meifang Yin, Yongming Li, **Jun Wu**. Burn wound assessment system using near-infrared hyperspectral imaging and deep transfer features. Infrared Physics & Technology. 2020. 111. 107-115

14. Yuzhen Wang, Ubaldo Armato, **Jun Wu**. Targeting tunable physical properties of materials for chronic wound care. Frontiers in bioengineering and biotechnology. 2020 8:584

15. Lijun Zhang, **Jun Wu**, Alfredo Ronca. In vitro and in vivo biocompatibility and inflammation response of methacrylated and maleated hyaluronic acid for wound healing. RSC Advances. 2020.08.

16. Mingzhou Yuan, Meifang Yin, Lijun Zhang, Jinghao Feng, Junyou Zhu, Ziheng Zhou, Bin Shu, Fei Zhou, Fangyingnan Zhang, Hanxiao Yin, Xiaoyan Wang, Shaohai Qi, **Jun Wu**. Selective debridement of burn wounds using hydrosurgery system. Int Wound J. 2020 Apr; 17:300-309.

2. Abbreviations

3D	Three-dimensional
LDI	Laser Doppler Image
SFDI	Spatial-Frequency Domain Imaging
LSI	Laser Speckle Imaging
OCT	Optical Coherence Tomography
IGG	Indocyanine Green
THz	Tera Hertz
SVR	Support Vector Regression
CNN	Convolutional Neural Network
CCD	Charge Coupled Device
LCTF	Liquid Crystal Tunable Filter

3. Informed Consent Form

Informed Consent Form

Project Title: Single-center clinical study based on self-developed near-infrared spectroscopy for exact diagnosis of burn wound depth.
Version of Informed Consent: 3.0, May 11, 2020
Project Leader: Jun Wu

Dear Patient,
You are invited to take part in the above clinical study. This Informed Consent Form provides you with the essential information to help you decide whether to take part in it or not. Please read it carefully and ask any questions to the researchers responsible for the study. Your participation is voluntary. This study has been approved by the Ethics Review Committee of this institution.

1. *Purpose of the Study*: Accurately figuring out the range and depth of burn injuries remains a significant challenge in wound management. Underestimating burn depth results in post-debridement residual necrotic tissue, while overestimating leads to the mistaken removal of viable tissue, causing a delayed or failed wound repair. This project intends to achieve precisely measurements of burn depth by using a near-infrared spectroscopy imager, and stands for the first international, objective, and data-based diagnosis of burn depth. It will validate a non-invasive, contact-free, and fast diagnostic technique advanccing an effective burn treatment. This method will radically replace existing subjective diagnostic methods, setting up a new international burn diagnostic paradigm.

2. *Research Procedure*: This study will involves a single-center self-control clinical study conducted in the First Affiliated Hospital of Shenzhen University, expecting to include 130 burnt patients. Through this clinical study, visible and near-infrared spectroscopy data from burn wounds will be collected, and further analyzed by building digital models and deep learning, aiming to set up a new international precise diagnostic standard, Standard Operating Procedure, and global burn treatment guidelines based on objective data. If you agree to join, we will conduct a clinical assessment of your wound, collect spectral data, take photos, and conduct a pathological examination of biopsy samples on the day of surgery. We will also

record your medical progress and treatments. The study will categorize based on pathological results, which will not affect your treatment plan or outcome. No long-term study follow-up will be needed .

3. *Risks and Discomforts*: Near-infrared light, a portion of the natural light spectrum, will be used. The scanning probe will need no contact, take approximately one minute, and will not further damage your wound. The study will collect your tissue biopsy samples, and their collection will be conduceted by strictly aseptic technique. Complications due to the biopsy may include mild pain, , local bleeding, redness and swelling, infection, delayed wound healing, and scar formation. If any of these occur, symptomatic treatment will be provided, whose costs are borne by the researchers.

4. *Benefits:* Taking part in this study will not directly benefit you, but your participation might contribute to the development of novel burn wound diagnostic methods.

5. *Associated Costs:* The study will only collect biopsied tissue samples during surgery, incurring in no added costs or time for you.

6. *Privacy Concerns:* If you decide to take part, all your personal data and study information will remain confidential. Spectroscopy data and skin samples will be labeled with a research number, but remain anonymous. Identifiable information will not be shown to members outside the research team without your consent. All researchers and sponsors are bound to confidentiality. Your files will be stored in a locked cabinet, accessible only to researchers. Ethics Committee members may review your personal data at the research unit, ensuring compliance. Published study results will not disclose any personal data of yours.

7. *Compensation of injuries due to this study:* Should any harm related to this clinical study occur, you are entitled to free treatment and/or compensation under the standing Chinese law.

You can choose not to participate or you can notify researchers that you wish to withdraw at any time. Your data will not be included in the study, and your medical

treatment and rights will not be affected. On the other hand, researchers may terminate your participation if you require other treatments, do not follow the study plan, suffer study-related harm, or for any other good reason. You can inquire about the study progress and information anytime. For study-related questions, discomforts, injuries, or concerns about participant rights, contact Dr. Yating Wei at 18669051221.

Informed Consent Signature Page:

I read this informed consent form.

I had the opportunity to ask questions, and all have been answered.

I understand that participating is voluntary.

I can choose not to participate or notify researchers at any time my withdrawal without facing discrimination or retaliation. My medical treatment and rights will not be affected.

If I need other treatments, or do not follow the study plan, or suffer study-related injuries, or for any other reason, the researchers can terminate my participation.

I will receive a signed copy of the "Informed Consent Form."

Participant's Name: _____

Participant's Signature: _____

Date: _____ Year _____ Month _____ Day

Through this document I accurately informed the study candidates. . They read the informed consent form, had the opportunity to ask questions, and accepted to participate voluntarily.

Researcher's Name: _____

Researcher's Signature: _____

Date: _____ Year _____ Month _____ Day

(Note: If the participant is illiterate, a witness signature is required. If the participant is incapacitated, a representative's signature is needed.)